Sensor Applications

Wearable Sensing in Low-Field (0.55T) MRI Environment

Felix Muñoz[1,2,3], Krishna S. Nayak[1,2,*], and Yasser Khan[2,3,**]

[1] *Alfred E. Mann Department of Biomedical Engineering, University of Southern California, Los Angeles, CA, USA*
[2] *Ming Hsieh Department of Electrical and Computer Engineering, University of Southern California, Los Angeles, CA, USA*
[3] *The Institute for Technology and Medical Systems, Keck School of Medicine, University of Southern California, Los Angeles, CA, USA*
[*] *Fellow, IEEE,* [**] *Senior Member, IEEE*

Abstract—Wearable sensors in the magnetic resonance imaging (MRI) environment enable the use of wearable devices to monitor vital signs such as heart rate, respiration rate, blood pressure, temperature, and biochemical markers during an MRI scan. Here, we demonstrate the efficacy of Bluetooth Low Energy (BLE)-enabled optical photoplethysmogram (PPG) sensors at a low-field MRI strength of 0.55 Tesla. We evaluate the noise in a wearable device caused by eddy currents from the rapidly switching MRI gradients, as well as the MRI noise and artifacts introduced by the BLE wearable into the MR receiver. Our results show that a custom-made BLE PPG sensor can operate effectively during 0.55T MRI scanning, providing precise (within 20ms) wireless monitoring of PPG with no observable effect on either the sensor signal or image quality. These results are encouraging for future wearable sensing in the MRI environment.

Index Terms—wearable electronics, MRI-compatible wearables, low-field MRI.

I. INTRODUCTION

The development of wearable sensors is an emerging technology that has significantly improved the ability to monitor physiological signals while reducing discomfort for subjects [1]. These sensors are used to detect clinically relevant signals such as heart rate [2], body temperature [3], blood oxygen saturation [4], and cardiac signals like electrocardiograms (ECG) [5]. This technology includes wearable garments [6], wearable ECG devices [7], wristbands [8], watches [9], and rings [10]. Using these devices during an MRI procedure is desirable as they provide continuous, real-time monitoring of vital physiological parameters while ensuring patient comfort due to their wearable form factor [11]. MRI-compatible wearable sensing is particularly valuable for interventional MRI [12]–[14], where real-time physiological assessment is essential for patient safety monitoring.

Despite the aforementioned advantages, most commercially available devices cannot be employed during MR imaging due to compatibility issues. The electromagnetic emissions from the MR scanner often induce unintended eddy currents in these devices when subject to the encoding gradients and radiofrequency fields used for excitation. [15]. These induced currents can be picked up by the device's circuit elements, and cause distortions in the true signal. The use of circuits, such as receivers and amplifiers, has already been shown to work inside the MRI environment, if they are designed correctly [16], [17]. Bluetooth Low Energy (BLE) enables wireless data transmission with low energy consumption allowing it to be embedded in small wearable devices with small batteries, well suitable for wearable health technology [18]. BLE has been previously shown to operate satisfactorily inside the MR environment, specifically at 3T [19], [20] and at the ultra-low field strength of 0.178T [21]. Note that the evaluation at 0.178T utilized a dedicated extremity MR scanner, which did not utilize high slew rates, and consequently, the changing flux of the gradients was less likely to induce strong eddy currents in the device. This work seeks to address this gap by evaluating the compatibility of BLE within a 0.55T scanner equipped with high-performance gradients and high slew rates. This analysis

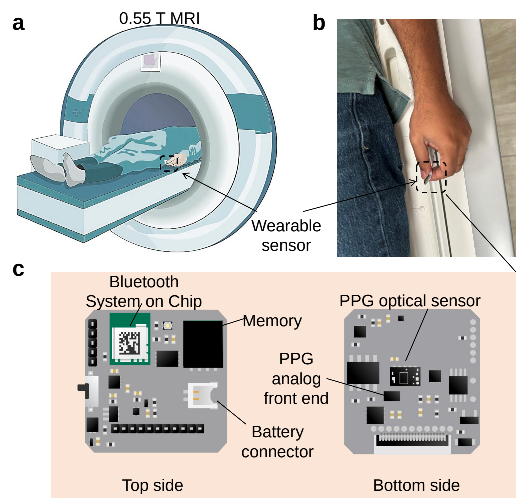

Fig. 1. **Wearable sensor placement and positioning within the 0.55T MRI environment**. (**a**) Positioning of the wearable during scanning. (**b**) The sensor is placed under the left index finger of the volunteer. (**c**) The optical PPG sensor and circuit board components are shown. The PPG sensor is interfaced with a Nordic nRF52832 system-on-chip, which streams data to a phone application.

will offer a detailed assessment of BLE's compatibility for wireless data transmission inside the MR environment, especially under high slew rate conditions. Additionally, it will examine the impact of BLE on the induced noise levels in the MR scanner, which is critical given the inherently lower signal-to-noise ratio (SNR) associated with < 1.5T MRI systems.

In this work, we evaluate the performance of a custom-made, handheld, small (25 mm x 25 mm), and low-cost (< $100) wearable BLE device inside the MR environment. We observe identical cardiac pulse signals from the wearable and the MRI scanner's measurement system, validating the wearable's efficacy inside the MRI environment.

II. METHODS

The proposed device is shown in Fig. 1. A reflection-type photoplethysmograph (PPG) sensor is used. The optical sensor,

Corresponding author: Yasser Khan (e-mail: yasser.khan@usc.edu).

SFH 7050 (OSRAM), is interfaced with the nRF52832 Bluetooth transceiver via a serial peripheral SPI interface [22], [23]. Red (660 nm) and NIR (950 nm) lights are used to collect PPG signals at a 50 Hz sampling frequency. A silicon photodiode of the SFH 7050 sensor collects the reflection-mode optical signal. The device is powered by a rechargeable lithium-polymer battery (3.7V, 80mAh), which provides about 8 hours of continuous use in MRI settings. The wearable sensor is designed with a small and ergonomic form factor to be comfortably hand-held without the need for any affixing mechanisms. This design ensures consistent placement during measurements while leveraging the hand's typical position away from isocenter.

The custom-made wearable acquires heart rate from the PPG signal and measures skin temperature. The PPG and temperature data are transferred using BLE technology to a compatible smartphone, which displays these measurements in real time. Due to the lower magnetic attraction forces in low-field MRI, the smartphone can be safely placed in a corner of the room, outside of the 5-Gauss field line. The wearable's performance is compared to the optical plethysmograph measurements of the Physiological Measurement Unit (PMU) of the scanner. This reference sensor, typically used to acquire electrocardiogram or PPG signals for cardiac and respiratory gating, is MRI-compatible.

The system overview of the custom-made wearable sensor is shown in Fig. 1c. The operation of the wearable is evaluated on a 0.55T MRI system (prototype MAGNETOM Aera, Siemens Healthineers, Erlangen, Germany) equipped with high-performance gradients (45 mT/m amplitude, 200 T/m/s slew rate). We performed a comprehensive evaluation of the compatibility of the custom-made wearable inside the MR environment, encompassing three key aspects. First, we evaluated the impact of induced noise on the wearable due to the changing magnetic fields produced by the scanner. Second, we assessed the converse effect, determining if the BLE emissions from the wearable create additional noise in the MR receiver. Finally, to assess the wearable's operation in a real-world setting, we tested its performance during the scanning process by collecting PPG data and comparing it with the Siemens PMU sensor. The PPG signals from both sensors were obtained from a healthy volunteer, who provided written informed consent under a protocol approved by our Institutional Review Board.

A. Evaluation of the Induced Noise on the Wearable

MRI imaging relies on the use of imaging gradients for spatial encoding. These gradients are superimposed on the main magnetic field and effectively shift the resonance frequency of the spins temporally and spatially. Since these gradients are switched on and off up to several hundred times every second, they can cause interference in nearby electronics by electromagnetic induction. The rapidly changing magnetic flux created by these gradients through the closed electrical paths of nearby circuits causes opposing currents to flow [24]. In our case, these currents can combine with the photodiode currents and contribute additional noise.

To evaluate the noise introduced by the imaging gradients and the excitation RF fields on the custom-made wearable, the wearable is placed on a water phantom, as shown in Fig. 2a. As the sensor is operated in reflection mode, the water does not reflect light back to the photodiode, thus only noise is obtained. The imaging sequence consists of multiple 2D gradient echo sequences (GRE) with resolutions 1x1x2 mm^3 to 1x1x4 mm^3, TR = 10 ms, TE = 4.62 ms, and readout bandwidth of 130 Hz/Pixel. While the scan is underway, the wearable transmits data via BLE to the smartphone located in the corner of the room.

B. Evaluation of the Induced Noise on the MR Scan by the Wearable

The ferromagnetic materials inside the wearable distort the static magnetic field. These distortions appear as signal voids in MRI images. To evaluate these distortions, the above setup shown in Fig. 2a is used to obtain an image with the wearable attached to a water bottle, and the acquired signal void area is analyzed. Since there can also be interference by the BLE module with the MR receiver, an image is obtained where the wearable is placed at the lower end of the phantom, and this image is obtained again, but with the MR wearable removed. The receiver noise is then compared in both cases to assess if there is an effect from the BLE module.

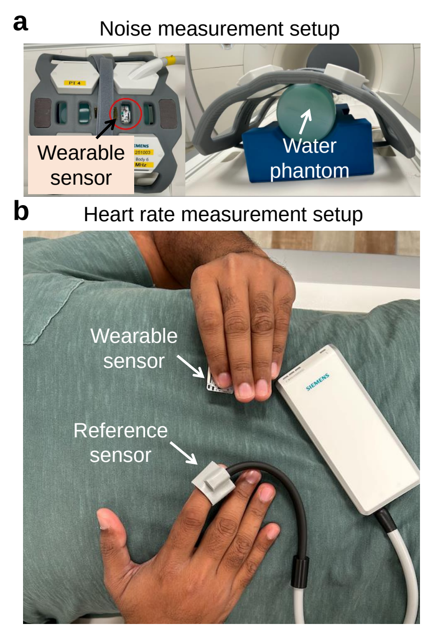

Fig. 2. **Wearable sensor testing in the MR environment**. (**a**) Setup for evaluating induced noise on the sensor caused by the MR gradients and RF excitation pulses, as well as the noise induced in the MR receiver by the wearable. The red circle indicates the location of the wearable above the water phantom. (**b**) Setup for validating heart rate measurements using the wearable sensor alongside the scanner's reference PMU sensor.

C. Wearable Sensor Operation During MRI

The operation of the wearable during MRI scanning is evaluated against the performance of the reference MR-compatible PMU sensor. The wearable sensor is held in the left hand between the index and thumb, while the reference sensor is placed on the right index finger. This setup is illustrated in Fig. 2b. While simultaneously recording data from both sensors, an MR image of the spine is obtained. To evaluate operation during high gradient slew rate sequences, such as spiral imaging [25], a service sequence where the magnetic field encoding gradients amplitude rises from 0 to the maximum amplitude at a high slew rate is also performed during acquisition. The raw PPG signals from both sensors are filtered with a 0.3-2.5 Hz bandpass filter. Temporal alignment of both PPG signals is evaluated, and heart rate (HR) is extracted by calculating peak-to-peak duration for every heartbeat based on the peak detection algorithm by Python's Peakdet [26]. The accuracy of the sensor's HR measurements relative to the reference sensor was evaluated using the root mean square error (RMSE) as follows: RMSE = $\sqrt{\frac{1}{n}\sum_{i=1}^{n}(y_i - \hat{y}_i)^2}$, where y_i is the reference sensor's HR, $\hat{y}_i$ is the wearable sensor's HR, and n is the number of samples.

III. RESULTS

A. Evaluation of the Induced Noise on the Wearable

Noise measurements obtained from the wearable attached to the water phantom during imaging are shown in Fig. 3. Areas that are shaded gray represent the time of active scanning. There was no observed increase in the noise during the imaging process. The lack of increased noise during scanning, including during the RF excitation pulse, is due in part to the lower excitation power requirements of lower field strengths [27].

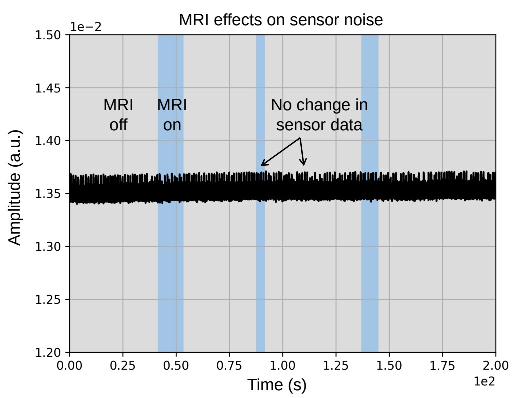

Fig. 3. **Effect of the MR magnetic field gradients and RF excitation energy on the wearable noise level**. The black bar indicates the obtained noise values and the blue shaded areas indicate areas of slewing gradients. The blue segment indicates the periods when the MRI scanner is active; the initial part (~ 3 ms)corresponds to RF excitation, while the remainder represents the periods where the gradients are slewing or maintaining a constant state. There is no observed variation in the noise level of the wearable inside the MR environment, even in areas where the gradients are slewing. Note that signal amplitude is reported in arbitrary units because it depends on device- and subject-specific factors, with the focus being on relative peaks and troughs that indicate pulse activity.

B. Evaluation of the Induced Noise on the MR Scan by the Wearable

The MR signal loss resulting from the ferromagnetic materials inside the wearable is shown in Fig. 4a. There is a 15 mm signal void as measured from the surface of the phantom, where the sensor is placed. The results of the influence of the Bluetooth transmission on the MR receiver are shown in Fig. 4b. There were no visible changes in the images, and the profile of the image across the cross-section did not show a change in noise level. Dark areas in the corners of the image were used to analyze the noise variance relative to the maximum signal amplitude. With the sensor active, this variance was 0.82%, and 0.83% without. This indicates that Bluetooth transmission does not significantly affect MR receiver noise.

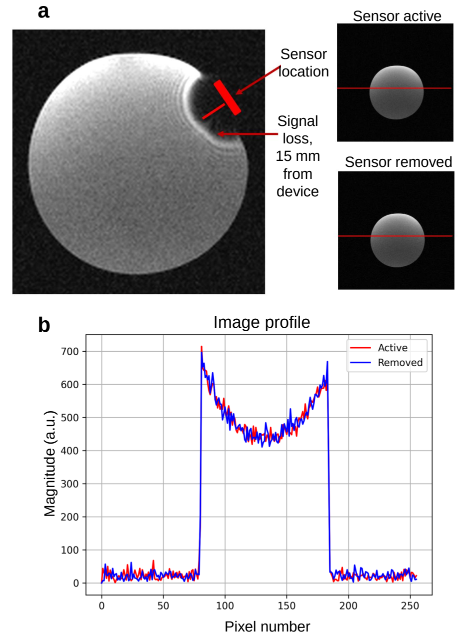

Fig. 4. **Effects of the wearable sensor on MR images**. (**a**) Signal loss due to ferromagnetic materials in the wearable casing, with a 15 mm signal loss from the device location. (**b**) Reconstructed images with the sensor active and with the sensor removed. No visible differences are observed in the reconstructed images or in the image profile, as shown in the profile view. The Imaging parameters were: Resolution = 1 x 1 x 2 mm^3 , TR = 10 ms, TE = 4.62 ms, and readout bandwidth of 130 Hz/Pixel. Note that pixel values are reported in arbitrary units because it depends on device- and subject-specific factors, with the focus being on relative contrast rather than absolute values.

C. Wearable Sensor Operation During MRI

Recorded PPG waves from both sensors during MR scanning are shown in Fig. 5a. The blue shaded areas indicate slewing gradients due to MR imaging. The expected PPG wave is visible on both sensors, with excellent alignment between the detected peaks. The time difference between detected peaks ($T_{BLE} - T_{REF}$) was 20.2 ms (mean) ± 13.8 ms (standard deviation). The calculated heart rates from both sensors are shown in Fig. 5b. The heart rate from the wearable exhibits less than 2.15 beats per minute (bpm) RMSE compared to the reference sensor.

IV. CONCLUSION

We demonstrate that a custom-made wearable sensor can operate effectively during 0.55T MRI scanning, with no observable effect on either the sensor signal or image quality. This allows accurate and precise (within 20ms) wireless monitoring of cardiac pulse waves during MR scans, even at high slew rates. There was an observed signal loss of 15 mm from the location of the wearable. This does not pose a problem as long as the sensor is positioned at least 15 mm away from the target imaging region. As the wearable is designed to be held in either hand, this signal void is unlikely to pose a problem in most clinical scenarios. For instance, during imaging of the hand, the sensor can be held in the opposite hand. While the sensor was not affected by the magnetic field gradients of the MR environment, it exhibited high sensitivity to hand motion. Additionally, flickering light from room fixtures interfered with the PPG signal, adding noise.

This article has been accepted for publication in IEEE Sensors Letters. This is the author's version which has not been fully edited and content may change prior to final publication. Citation information: DOI 10.1109/LSENS.2025.3528305

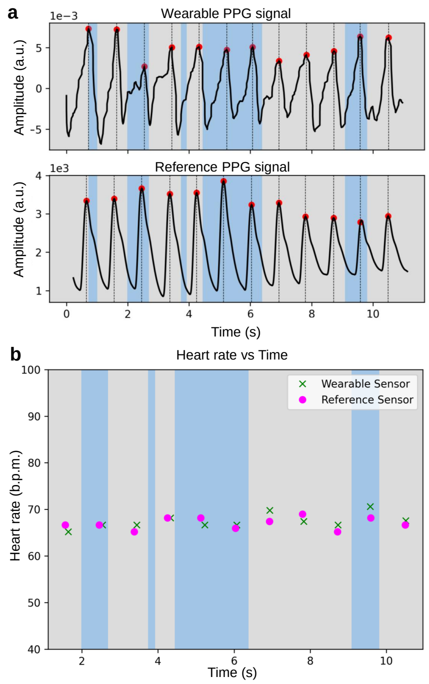

Fig. 5. **PPG and heart rate measurements from the wearable and reference sensors**. (**a**) The top graph shows the wearable PPG, and the bottom graph shows the reference PPG. The PPG waves are clearly visible, with detected peaks from both sensors aligned within 20.2 ms ± 13.8 ms. (**b**) The heart rate measured during an MR scan, obtained from the peak locations shown in a. The RMSE of the wearable sensor with respect to the PMU reference sensor is less than 2.15 bpm. The blue shaded areas indicate times when the magnetic field gradients are slewing.

The observed 20.2 ms bias between detected peaks is likely due to a delay in timestamp generation by the mobile device. The next steps are to address these issues for more seamless operation of the sensor.

ACKNOWLEDGMENT

This work was supported in part by USC Zumberge Preliminary Studies Research Award.

REFERENCES

[1] S. C. Mukhopadhyay, "Wearable sensors for human activity monitoring: A review," *IEEE sensors journal*, vol. 15, no. 3, pp. 1321–1330, 2014.

[2] Y. Khan, M. Garg, Q. Gui, M. Schadt, A. Gaikwad, D. Han, N. A. Yamamoto, P. Hart, R. Welte, W. Wilson *et al.*, "Flexible hybrid electronics: Direct interfacing of soft and hard electronics for wearable health monitoring," *Advanced Functional Materials*, vol. 26, no. 47, pp. 8764–8775, 2016.

[3] W. Honda, S. Harada, T. Arie, S. Akita, and K. Takei, "Printed wearable temperature sensor for health monitoring," in *SENSORS, 2014 IEEE*. IEEE, 2014, pp. 2227–2229.

[4] Y. Khan, D. Han, J. Ting, M. Ahmed, R. Nagisetty, and A. C. Arias, "Organic multi-channel optoelectronic sensors for wearable health monitoring," *IEEE Access*, vol. 7, pp. 128 114–128 124, 2019.

[5] P. Kamga, R. Mostafa, and S. Zafar, "The use of wearable ECG devices in the clinical setting: a review," *Curr Emerg Hosp Med Rep*, vol. 10, no. 3, pp. 67–72, 2022.

[6] R. Villar, T. Beltrame, and R. L. Hughson, "Validation of the hexoskin wearable vest during lying, sitting, standing, and walking activities," *Applied Physiology, Nutrition, and Metabolism*, vol. 40, no. 10, pp. 1019–1024, 2015. [Online]. Available: https://doi.org/10.1139/apnm-2015-0140

[7] A. Hall, A. R. J. Mitchell, L. Wood, and C. Holland, "Effectiveness of a single lead alivecor electrocardiogram application for the screening of atrial fibrillation: A systematic review," *Medicine*, vol. 99, no. 30, p. e21388, Jul 2020.

[8] J. Dieffenderfer, H. Goodell, B. Bent, E. Beppler, R. Jayakumar, M. Yokus, J. Jur, A. Bozkurt, and D. Peden, "Wearable wireless sensors for chronic respiratory disease monitoring," in *2015 IEEE 12th International Conference on Wearable and Implantable Body Sensor Networks (BSN)*. IEEE, 2015, pp. 1–6. [Online]. Available: http://ieeexplore.ieee.org/document/7299411/

[9] C. C. Cheung, A. D. Krahn, and J. G. Andrade, "The emerging role of wearable technologies in detection of arrhythmia," *Canadian Journal of Cardiology*, vol. 34, no. 8, pp. 1083–1087, 2018.

[10] R. Cao, I. Azimi, F. Sarhaddi, H. Niela-Vilen, A. Axelin, P. Liljeberg, and A. M. Rahmani, "Accuracy assessment of oura ring nocturnal heart rate and heart rate variability in comparison with electrocardiography in time and frequency domains: comprehensive analysis," *Journal of Medical Internet Research*, vol. 24, no. 1, p. e27487, 2022.

[11] Y. Khan, A. E. Ostfeld, C. M. Lochner, A. Pierre, and A. C. Arias, "Monitoring of vital signs with flexible and wearable medical devices," *Advanced materials*, vol. 28, no. 22, pp. 4373–4395, 2016.

[12] A. E. Campbell-Washburn, R. Ramasawmy, M. C. Restivo, I. Bhattacharya, B. Basar, D. A. Herzka, M. S. Hansen, T. Rogers, W. P. Bandettini, D. R. McGuirt *et al.*, "Opportunities in interventional and diagnostic imaging by using high-performance low-field-strength MRI," *Radiology*, vol. 293, no. 2, pp. 384–393, 2019.

[13] R. J. Lederman, "Cardiovascular interventional magnetic resonance imaging," *Circulation*, vol. 112, no. 19, pp. 3009–3017, 2005.

[14] A. Kolandaivelu, C. G. Bruce, F. Seemann, D. K. Yildirim, A. E. Campbell-Washburn, R. J. Lederman, and D. A. Herzka, "Evaluation of 12-lead electrocardiogram at 0.55 T for improved cardiac monitoring in magnetic resonance imaging," *Journal of Cardiovascular Magnetic Resonance*, vol. 26, no. 1, p. 101009, 2024.

[15] M. A. Secretariat, "Patient monitoring system for MRI," *Ontario Health Technology Assessment Series*, vol. 3, no. 7, pp. 1–16, 2003. [Online]. Available: http://www.health.gov.on.ca/ohtas

[16] J. Reber, J. Marjanovic, D. Brunner, A. Port, T. Schmid, B. Dietrich, U. Moser, C. Barmet, and K. Pruessmann, "An in-bore receiver for magnetic resonance imaging," *IEEE Transactions on Medical Imaging*, vol. 39, no. 4, pp. 997–1007, 2020.

[17] B. Sporrer, L. Wu, L. Bettini, C. Vogt, J. Reber, J. Marjanovic, T. Burger, D. Brunner, K. Pruessmann, G. Troster *et al.*, "A fully integrated dual-channel on-coil CMOS receiver for array coils in 1.5-10.5 T MRI," *IEEE Transactions on Biomedical Circuits and Systems*, vol. 11, no. 6, pp. 1245–1255, 2017.

[18] J. Tosi, F. Taffoni, M. Santacatterina, R. Sannino, and D. Formica, "Performance evaluation of bluetooth low energy: A systematic review," *Sensors*, vol. 17, p. 2898, 2017. [Online]. Available: https://doi.org/10.3390/s17122898

[19] C. Vogt, J. Reber, D. Waltisberg, L. Buthe, J. Marjanovic, N. Munzenrieder, K. Pruessmann, and G. Troster, "A wearable bluetooth le sensor for patient monitoring during MRI scans," in *Proceedings of the Annual International Conference of the IEEE Engineering in Medicine and Biology Society, EMBS*, 2016, pp. 4975–4978.

[20] B. Silemek, V. Acikel, C. Oto, A. Alipour, Z. Aykut, O. Algin, and E. Atalar, "A temperature sensor implant for active implantable medical devices for in vivo subacute heating tests under MRI," *Magnetic Resonance in Medicine*, vol. 79, no. 5, pp. 2824–2832, 2018.

[21] J. Pribil, A. Přibilová, and I. Frollo, "Wearable PPG sensor with bluetooth data transmission for continual measurement in low magnetic field environment," in *International Conference on Applied Electronics*, ser. September, vol. 2021. IEEE Computer Society, 2021.

[22] Y. Khan, M. Mauriello, P. Nowruzi, A. Motani, G. Hon, N. Vitale, J. Kim, A. Foudeh, D. Duvio, E. Shols *et al.*, "Design considerations of a wearable electronic-skin for mental health and wellness: balancing biosignals and human factors," *bioRxiv*, 2021.

[23] Y. Khan, M. L. Mauriello, P. Nowruzi, A. Motani, G. Hon, N. Vitale, J. Li, J. Kim, A. Foudeh, D. Duvio *et al.*, "On stress: Combining human factors and biosignals to inform the placement and design of a skin-like stress sensor," 2024.

[24] P. Düppenbecker, B. Weissler, P. Gebhardt, D. Schug, J. Wehner, P. Marsden, and V. Schulz, "Development of an MRI-compatible digital sipm detector stack for simultaneous PET/MRI." *Biomed Phys Eng Express*, vol. 2, no. 1, p. 015010, 2016.

[25] S. Lingala, Y. Zhu, Y. Lim, A. Toutios, Y. Ji, W. Lo, N. Seiberlich, S. Narayanan, and K. Nayak, "Feasibility of through-time spiral generalized autocalibrating partial parallel acquisition for low latency accelerated real-time MRI of speech," *Magnetic Resonance in Medicine*, vol. 78, no. 6, pp. 2275–2282, 2017.

[26] R. Markello and E. DuPre, "peakdet," https://github.com/rmarkello/peakdet, 2022, [Accessed 2022 Oct 31].

[27] T. S. Ibrahim and L. Tang, "Insight into RF power requirements and B1 field homogeneity for human MRI via rigorous FDTD approach," *Journal of Magnetic Resonance Imaging*, vol. 25, pp. 1235–1247, 6 2007.